RESEARCH ARTICLE

BON VIEW PUBLISHING

Study on the Separation Process of Non-Metallic Inclusions at the Steel-Slag Interface Using Water Modeling Under Static and Dynamic Conditions

Sajjad Muhammad[1], Xin Tao[1], Dekang Ren[1], Hongyu Zhang[1], Tao Liu[1] and Chao Chen[1],*

[1]College of Materials Science and Engineering, Taiyuan University of Technology, China

Abstract: Effective inclusion removal is essential for making high-quality steel. The inclusion separation into the slag involved a step of flow across the slag-steel interface in the steelmaking process. This research study examines how polypropylene (PP) and hollow Al_2O_3 particles float in water and oil interface to simulate the inclusion floating process. Both static and dynamic (with water flow) conditions are studied. The movement of particles of various sizes and densities in a rectangular acrylic container are recorded by a high-speed camera setup. The experiment utilized water, silicone oil, and particles of varying sizes and densities to investigate the impact of physical properties on floating dynamics. Results demonstrated that under high viscosity conditions, particles were unable to cross the water-oil interface, despite having reduced densities. However, due to their lower viscosity, PP particles were able to float on top of the silicone oil. Using silicone oil with a viscosity of 0.0288 Pa·s, 3.96 mm PP particles displaced 70% of dimensionless displacement, whereas 3.93 mm hollow Al_2O_3 particles displaced 100% of dimensionless displacement. Dynamic measurements revealed that larger 3.9 mm Al_2O_3 particles moved 75% of dimensionless displacement in 0.2 s, compared to 65% of dimensionless displacement for smaller 3.1 mm Al_2O_3 particles. The terminal velocities of 3.93 mm Al_2O_3 particles were 0.143 m/s and 3.12 mm particles were 0.135 m/s. This study allows steelmakers to improve the process and assure better separation of inclusions, resulting in stronger, more reliable steel products.

Keywords: water model, steel-slag interface, inclusion, motion behavior

1. Introduction

Non-metallic inclusions are sometimes harmful to steel product quality [1, 2]. Effective separation of inclusions from molten steel is critical for ensuring steel quality, as inclusions can negatively impact mechanical properties and performance. Many research papers have focused on the formation and control of inclusions during steelmaking process [3–11]. Absorption by slag [12–14] and adhesion to refractories are two common methods to remove inclusions.

The absorption of inclusion by the top slag can be divided into four steps [15]: (1) Inclusions are following the macroscopic flow and transported to the turbulent boundary layer of the steel-slag interface; (2) the boundary layer transports the inclusions to the steel-slag interface; (3) the inclusions separates to the slags; and (4) the slag phase dissolves the inclusions. These four steps have been studied in research papers separately: step 1 in references [5–10], step 2 in references [16–18], step 3 in references [19–24], and step 4 in references [12, 25–27].

Water modeling can be used to simulate the physical interactions and fluid movements that occur throughout the steelmaking process, for example, the study of inclusion behavior and separation at steel-slag interface [28–35]. The research status has been overviewed by Tao et al. [34]. An earlier work could be dated back to the research by Ferchichi and Duval in 2011, and the glycerol and silicone oil are used to study the slag and water phases. Besides, the millimeter polymer spheres are used to study inclusions. The hollow Al_2O_3 particles were used for modeling of inclusions by Liu et al. [29]. A comprehensive study was performed by Zhou et al. [30] in 2017, and the shape of size of particles, viscosity, and interfacial tension of oil are all investigated. Besides, inclusion particle clusters are studied by Zhu et al. [31, 32]. In 2024, Nishibata et al. [33] systematically studied the breakup and entrapment of particle at the steel-slag interface. In 2024, Tao et al. [34] studied the polypropylene (PP) and aluminum oxide particle separation in a static water model experiment. The factors affecting the movement of inclusions at the slag-steel interface were explored. Recently, Liu et al. [35] studied the inclusions flotation in gas-stirred ladle system.

Light oil or other viscous materials often represent the slag phase. This method provides significant new insights into the surface tension and hydrodynamic factors that influence the migration and separation of non-metallic inclusions from steel to slag. Over the years, numerous studies have investigated these processes. However, most of the studies are focused on a static steel-slag interface condition. In steelmaking process for example, ladles, tundishes, and molds, the steel-slag interface is dynamic with fluid flow.

*Corresponding author: Chao Chen, College of Materials Science and Engineering, Taiyuan University of Technology, China. Email: chenchao@tyut.edu.cn

This study aims to simulate the separation of non-metallic inclusions at the steel-slag interface using water modeling under both static and dynamic conditions. We investigate the impact of inclusion velocity, size, and slag viscosity properties, on the separation process.

2. Experimental Materials and Strategies

In this section, we briefly introduced water model experimental materials and data evaluation.

2.1. Water model experimental materials and data evaluation

This part is further divided into three subgroups. First is 2.1.1. Materials used during experiment, second is 2.1.2. Experimental steps followed, and lastly 2.1.3. Data evaluation using water modeling technique and different software.

2.1.1. Experimental material

The inclusion flotation research uses an experimental device that is a rectangular acrylic container measuring 1000 mm in length, 100 mm in width, and 600 mm in height. There is a particle release port with a diameter of 10 mm located 500 mm from the bottom and 400 mm from the top on both the left and right sides. Water inlet and outlet are available at each location. The device and camera setup can be seen in Figure 1. For more information on the materials used and their physical properties, refer to Table 1.

In this study, the Fuhuang Junda Company's Qianyanlang 5KF20 3000-frame high-speed camera was used for recording, and its motion analysis software was used for data processing. The experimental setup is illustrated in Figure 2.

The picture below is a real-life picture of this experiment. This is a water tank that can control the flow. During the experiment, the liquid surface can be controlled in two states: static and dynamic.

Figure 1
(a) Acrylic rectangular container; (b) High-speed camera

Table 1
Physical factors of the materials used in the experiment

Materials	Diameter mm	Density Kg m^{-3}	Surface tension Nm^{-1}	Viscosity Pa·s
Water	–	1000	0.0278	0.001
Silicon oil	–	960/963	0.021	0.288/0.096
Polypropylene	3.13–3.93	910	0.031	–
Hollow Al$_2$O$_3$	3.12–3.93	710	0.65	–

Figure 2
Experimental device diagram

The materials used in this experiment include water (density of 1000 kg/m^3, surface tension of 0.0728 N/m, viscosity of 0.001 Pa·s), silicone oil (viscosity of 0.0288 Pa·s and 0.0096 Pa·s), PP particles (with diameters of 3.13 mm and 3.96 mm, density of 910 kg/m^3, surface tension of 0.031 N/m), and hollow Al$_2$O$_3$ tiny pieces (with diameters of 3.12 mm and 3.93 mm, density of 710 kg/m^3, surface tension of 0.65 N/m). Even though the size ratio of the particles used in the experiment is larger than the actual inclusion size ratio, the experiment on floating of inclusions is a qualitative study of the rules of floating motion, which meets the requirements of the experiment.

2.1.2. Experimental steps

Begin by filling a rectangular container with pure water until the liquid level reaches 50 cm. Then, pour silicone oil with a thickness greater than 10 mm on top. Use a glass rod to carefully remove any bubbles on the container walls to prevent them from affecting camera shots. Let the container sit until all small bubbles at the water-oil interface vanish. Next, add water outside the container until the liquid level is higher than inside. Connect a water pump to a water storage bucket and fill it with water. To get started, turn on the fill light located behind the rectangular container and adjust the camera height so that it is level with the water-oil interface. Set the camera settings and use a glass rod to focus the camera. To prevent bubbles from entering the system when releasing particles, place a beaker filled with water at the bottom of the particle release port and add particles into the water through the port. Use the camera to record the movement of the particles near the interface, then save the video. Upload the video to the motion analysis software that comes with the camera, set up a coordinate system, calibrate the size, and use the target tracking feature to analyze how the position of the particles changes over time. Analyze the data on particle displacement from the motion analysis software, import it into Origin software, create a dimensionless displacement image, and calculate the velocity data

over time by calculating the displacement. Finally, import the data into Origin to generate an image displaying the terminal velocity.

2.1.3. Data evaluation

This experiment utilized the camera's analysis software to track targets in the video and determine the position of particles in each frame.

In the analysis and processing software, the frame just before the particle reaches the water-oil interface for the first time is used as the coordinate origin. The vertical distance between the particle and the coordinate origin in subsequent frames is considered the y-axis displacement, allowing us to determine the particle's position at the water-oil interface. Due to the dynamic flow state of the system in the experiment, the water-oil interface may fluctuate, causing the camera to have difficulty focusing accurately and leading to jumps in the particle analysis process. To improve the reliability of the experimental data, the average of four neighboring data groups was used for analysis to minimize errors. Figure 3 illustrates the movement of particles at the water-oil interface.

Figure 3
Displacement of particles at the water-oil interface
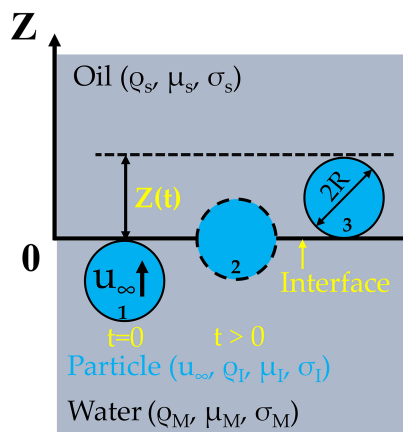
During the experiment, the size of the small particle was taken into consideration as it can impact the dimensionless displacement measurement. To address this, a dimensionless treatment was applied to the particle using the following calculation Equation (1):

$$Y = \frac{y}{L} \tag{1}$$

where (y) represents the actual displacement of the particle in the vertical direction, mm; (L) Particle diameter, mm; (Y) dimensionless displacement of the particle.

The experiment discovered that even though the particles are less dense than silicone oil, they are unable to move through the water-oil interface to reach the top of the oil layer. Instead, they tend to remain at the interface between the water and oil after some time. To further investigate this, videos of the particle movement within a specific timeframe were captured and analyzed.

2.2. Principle of movement and floating of inclusions

The numerical simulation method for studying the inclusion floating process is crucial in the field of steel smelting. By creating a precise numerical model, we can simulate the

movement, speed, and distribution of inclusions during smelting. This method allows for a better understanding of how inclusions float and provides valuable support for optimizing the process.

The similarity principle is categorized into static similarity and dynamic viscosity similarity. Static similarity principle considers the connection and wetting between inclusions, slag, and molten steel. To simulate the slag layer, liquid silicone oil is chosen due to its clear interface with water. By using liquid silicone oil as a substitute, particles can float to the oil layer and imitate the movement of inclusions at the steel-slag interface.

This experiment used water to represent molten steel, silicone oil to represent the slag film, solid PP particles of various sizes, and hollow Al_2O_3 particles to represent inclusions of different sizes. The goal was to make sure the oil layer had the right interface properties and dynamic viscosity similar to actual steelmaking slag.

$$\frac{\mu_w}{\mu_{st}} = \frac{\mu_0}{\mu_{sl}} \tag{2}$$

In the Equation (2) of dynamic viscosity of water, (μ_0) is dynamic viscosity of silicone oil; (μ_{st}) is dynamic resistance of liquid steel; (μ_{sl}) is dynamic viscosity of slag.

Based on reference [34], the dynamic viscosity of liquid steel slag ranges from 0.02 to 0.3 Pa·s, while molten steel has a viscosity of about 2 to 6.5×10^{-3} Pa·s. At a temperature of 20°C, water has a dynamic viscosity of approximately 1×10^{-3} Pa·s. The dynamic viscosity range of the silicone oil used in the simulation is calculated to be between 0.0031 and 0.15 Pa·s.

In this experiment, the silicone oil with the viscosity 0.0288 Pa·s and 0.0096 Pa·s, which falls within the acceptable range for viscosity similarity requirements, is used.

3. Experimental Results and Analysis of Floating Motion

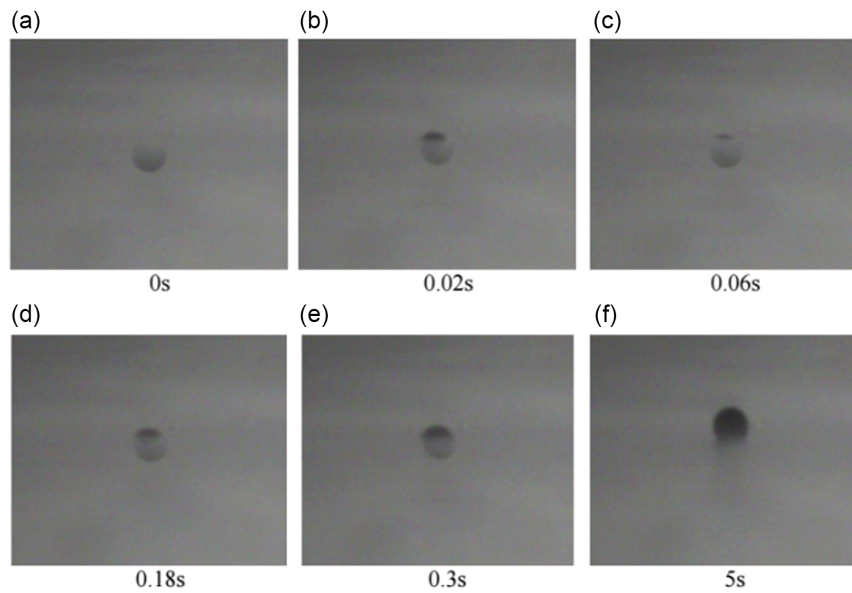### 3.1. Movement of particles at the water-oil interface

The image displayed is a snapshot from a video showing the movement of particles. In the video, we observed that even though the densities of PP particles and hollow Al_2O_3 particles are lower than that of silicone oil, they are unable to cross the water-oil boundary. As the particles approach the interface, it distorts and transforms their kinetic energy into elastic potential energy. Once all the kinetic energy is converted, the particles reach their maximum displacement in the y direction. Despite this, they have not crossed the interface yet and experience a rebound. Due to buoyancy, the particles gradually rise again but remain stuck at the water-oil interface for some time. Figures 4 and 5 depict small particles floating at the water-oil interface.

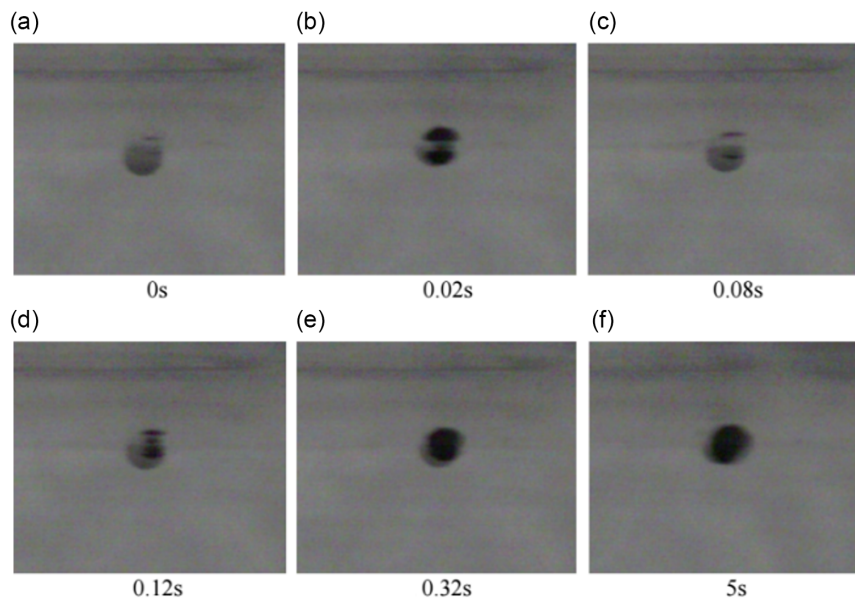### 3.2. Dimensionless displacement of particles

Experiments were conducted to study the factors influencing the final spot of tiny particles at the water-oil interface. Different-sized PP particles and hollow Al_2O_3 particles were used, along with silicone oil of varying viscosities. High-speed video and measurement software were used to capture and analyze particle movement. A coordinate system was established to track particle positions in each frame of the video. By converting pixel sizes to actual displacements, the motion of the particles was measured. To simplify the analysis, the position of the particle during motion is represented by a dimensionless displacement.

Figure 4
Photos of the movement of PP particles on the water-oil interference at different fractions of second

Figure 5
Photos of the movement of Al_2O_3 particles at the water-oil interface at different fractions of second

3.2.1. Static state results analysis of dimensionless displacement

Static state results analysis of dimensionless displacement in Figure 6 displays the dimensionless displacement diagrams of PP particles and hollow Al_2O_3 particles moving under silicone oil with a viscosity of 0.0288 Pa·s in a static environment. Under these conditions, the particles settle quickly. Both types of particles bounce back after hitting the water-oil interface and then float due to buoyancy. The diagram shows that hollow Al_2O_3 particles with a 3.93 mm diameter have a dimensionless displacement of around 1.0, while PP particles with a 3.96 mm diameter have a dimensionless displacement of about 0.7.

This experiment was performed with tiny particles in oil. It was observed how far 3.12 mm hollow Al_2O_3 particles and 3.13 mm PP particles moved in silicone oil with a viscosity of 0.0096 Pa·s when everything was in static state. In Figure 7, it can be observed that the hollow Al_2O_3 particles moved about 0.8 of dimensionless displacement, while the PP particles moved about 1.25 of dimensionless displacement. The silicone oil that was used was really thin, so the PP particles were able to move more easily. That's why the PP particles moved further than the hollow Al_2O_3 particles. The PP particles were even able to move through the oil and reach the top.

Figure 6
The dimensionless displacement diagrams of the motion of PP particles and Al$_2$O$_3$ particles under silicone oil with a viscosity of 0.0288 Pa·s under static conditions. (a) 3.93 mm Al$_2$O$_3$ particles, (b) 3.96 mm PP particles
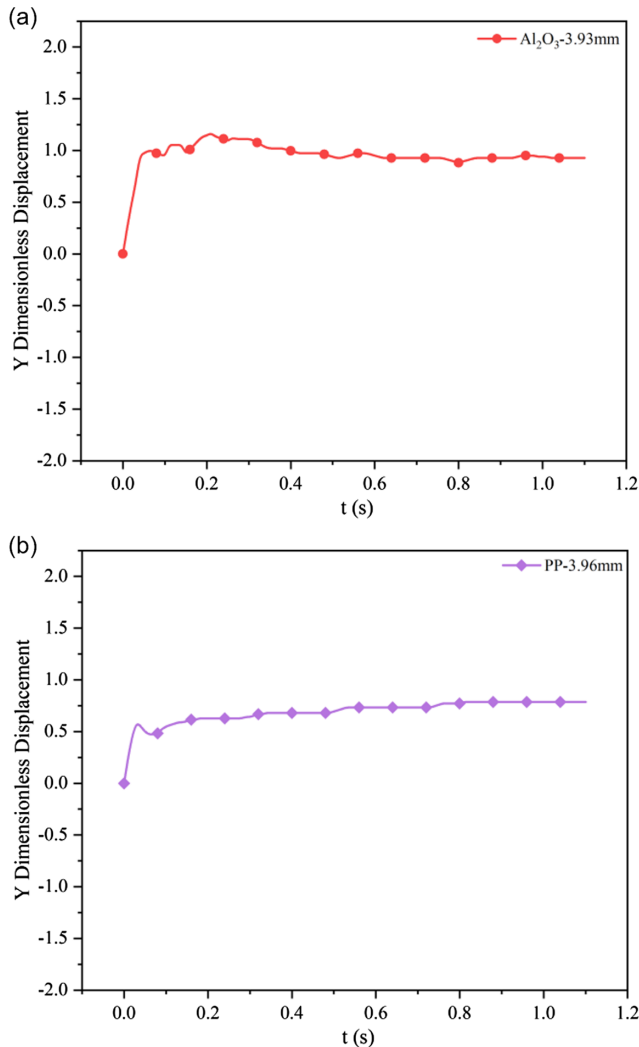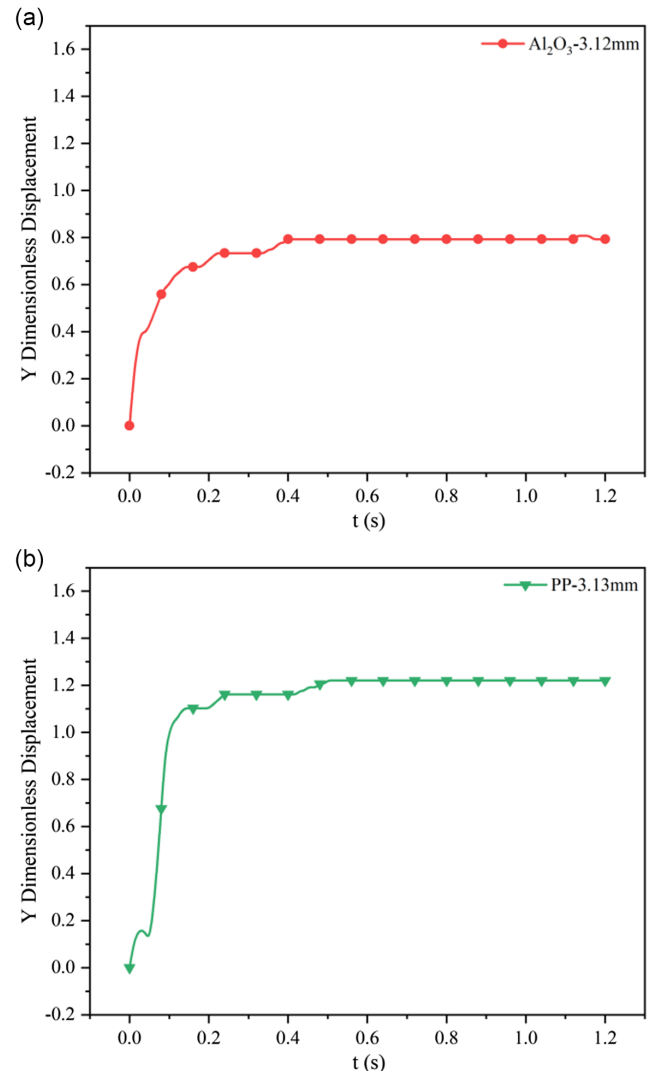

Figure 7
The dimensionless displacement of 3.12 mm hollow Al$_2$O$_3$ particles and the dimensionless displacement of 3.13 mm PP particles in silicone oil with a viscosity of 0.0096 Pa·s under static conditions. (a) 3.12 mm Al$_2$O$_3$ particles, (b) 3.13 mm PP particles

3.2.2. Dynamic state result analysis of dimensionless displacement

The dynamic state result analysis of dimensionless displacement is presented in Figure 8, which compares the movement of different-sized particles in water and oil. When 3.9 mm Al$_2$O$_3$ particles enter the water-oil interface, they move 0.75 of dimensionless displacement in 0.2 s. However, when 3.1 mm Al$_2$O$_3$ particles enter, they only move 0.65 of dimensionless displacement. The bigger the particle, the farther it moves. The same goes for PP particles; the 3.9 mm ones move 1.7 of dimensionless displacement, while the 3.1 mm ones only move 0.45 of dimensionless displacement. Bigger particles definitely travel further in this dynamic system. It can be argued that the size of the particles will affect the dimensionless displacement. The larger the particle's size, the greater its dimensionless displacement. However, since in a dynamic circulation system there will always be certain fluctuations at the interface, the particles will eventually stay on the water-oil interface and generate certain fluctuations along with the interface. Therefore,
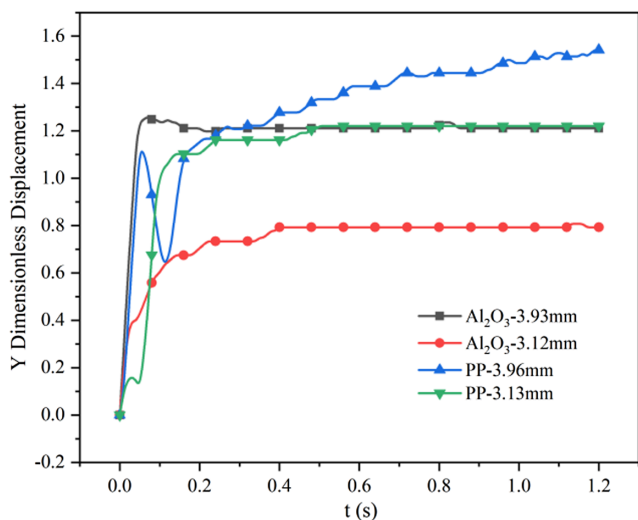
the tiny particles cannot always reach a stable state under dynamic conditions, and the dimensionless displacement of the end cannot reflect the influence of particle size on the movement of the tiny particles.
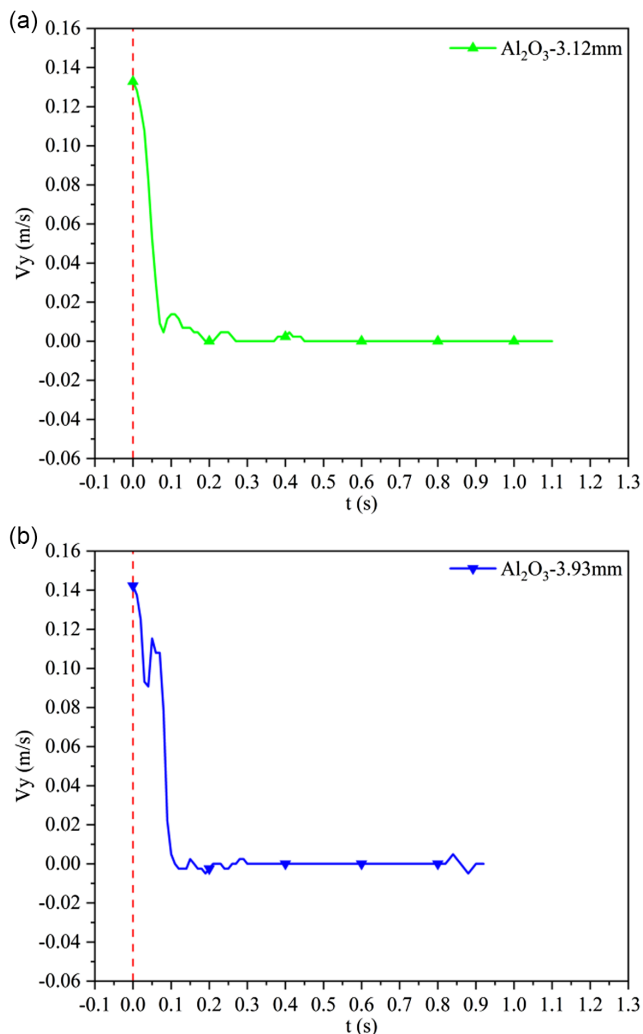
3.3. Terminal velocity of particles

To better understand how particles move while floating, we analyzed their velocity changes during this process. The velocity of the particle was determined by differentiating its actual displacement change as it floated upwards. In the resulting velocity curve, under static conditions, the particle reaches its maximum speed at 0 s before contacting the water-oil interface, which is known as the terminal velocity. Under dynamic conditions, this maximum speed occurs at 0.2 s before contacting the interface.

Figure 9 illustrates the terminal velocities of hollow Al$_2$O$_3$ particles of two different sizes in static water flow within silicone oil, which has a viscosity of 0.0096 Pa·s. The terminal velocity

Figure 8
Dynamic results of dimensionless displacement of Al$_2$O$_3$ particles and PP particles of different sizes

for hollow Al$_2$O$_3$ particles sized 3.12 mm is about 0.135 m/s, while for the same type particles sized 3.93 mm, it is approximately 0.143 m/s.

Figure 10 displays the terminal velocities of PP particles of two different sizes in static water flow within silicone oil, which has a viscosity of 0.0096 Pa·s. The terminal velocity for 3.13 mm PP particles is about 0.125 m/s, while for 3.96 mm particles, it is approximately 0.122 m/s.

In Figure 11, the comparison illustrates the terminal velocities of PP and hollow Al$_2$O$_3$ particles of similar types but varying sizes. The data reveal that the terminal velocity of 3.93 mm hollow Al$_2$O$_3$ particles exceeds that of 3.12 mm hollow Al$_2$O$_3$ particles. Similarly, the terminal velocity of 3.96 mm PP particles is higher than that of 3.13 mm PP particles. These findings indicate that, under static conditions at the silicone oil interface with a viscosity of 0.0096 Pa·s, larger particles experience greater terminal velocities compared to smaller particles of the same type.

Figure 12 illustrates velocity curves for PP particles and Al$_2$O$_3$ particles of varying sizes before and after their initial contact with the water-oil interface. Initially, buoyancy accelerates the particles

Figure 9
The terminal velocities of hollow Al$_2$O$_3$ particles of two different particle sizes under static water flow in silicone oil with a viscosity of 0.0096 Pa·s. (a) 3.12 mm Al$_2$O$_3$ particle, (b) 3.93 mm Al$_2$O$_3$ particle

Figure 10
The terminal velocities of PP particles of two different sizes under static water flow in silicone oil with a viscosity of 0.0096 Pa·s. (a) 3.13 mm PP particle, (b) 3.96 mm PP particle
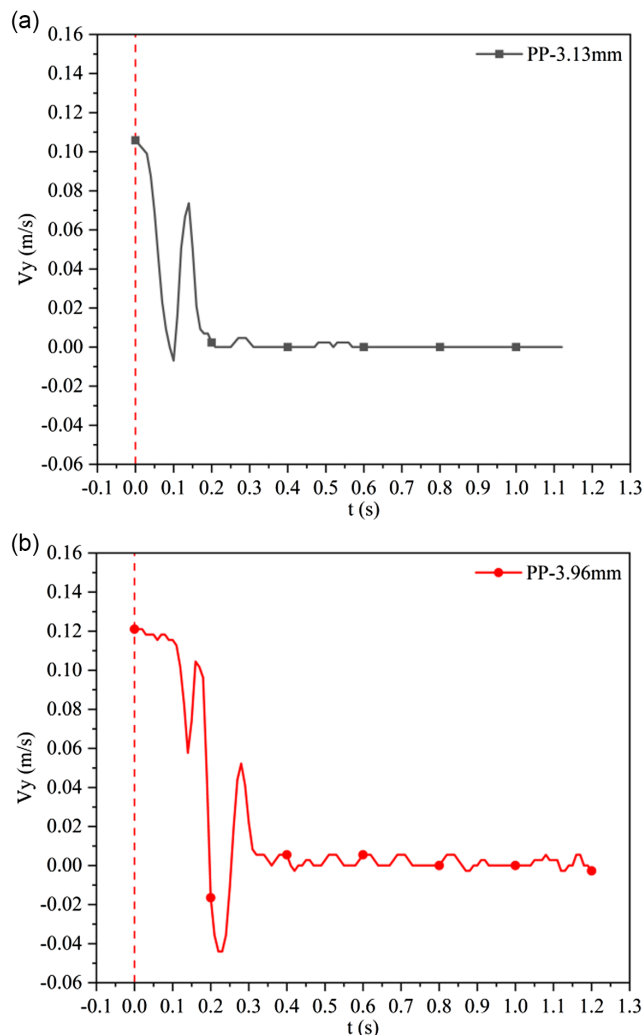
Figure 11
The comparison of terminal velocities of PP and hollow Al$_2$O$_3$ particles of the same type of particles with different particle sizes. (a) Hollow Al$_2$O$_3$ particles with different particle sizes, (b) PP particles with different particle sizes
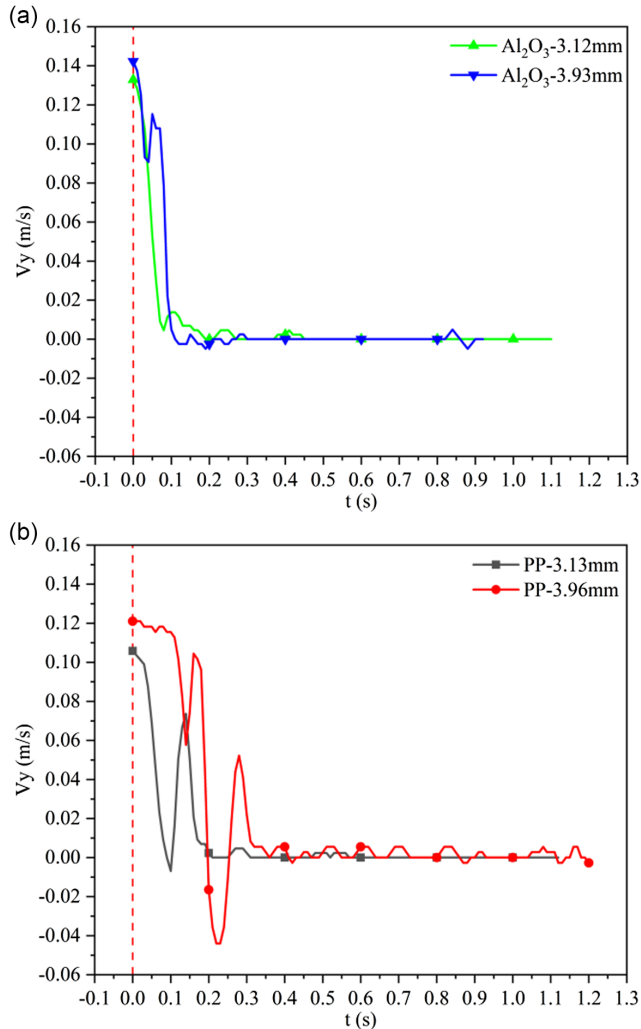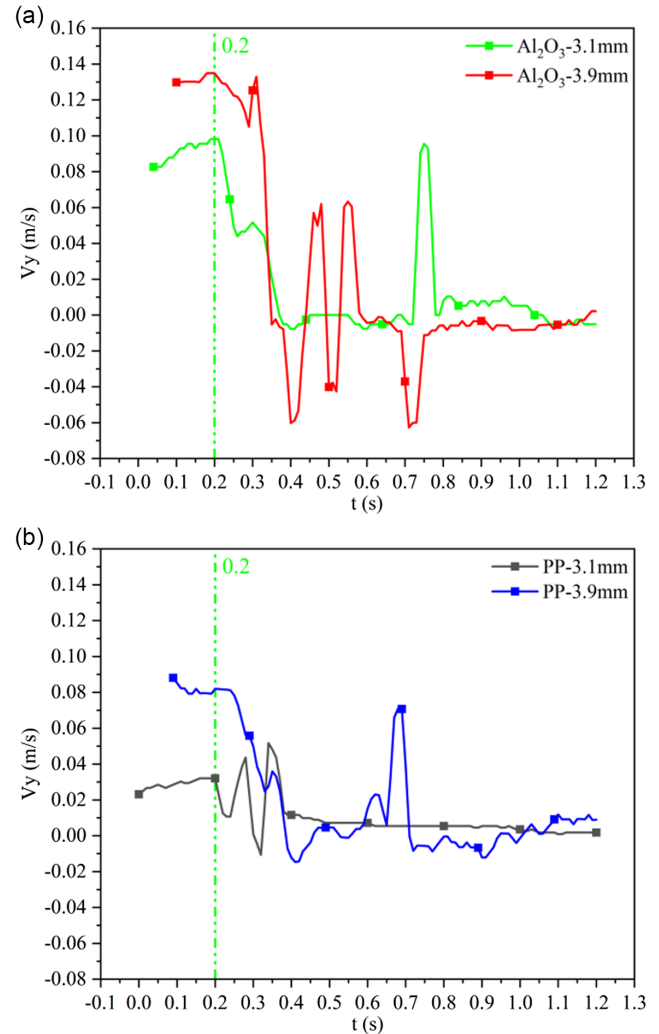

(a)

(b)

Figure 12
The comparison of the velocity curves of PP particles and Al$_2$O$_3$ particles of different sizes before and after the first contact with the water-oil interface (a) 3.1 mm and 3.9 mm Al$_2$O$_3$ particles, (b) 3.1 mm and 3.9 mm PP particles

(a)

(b)

towards the interface. As they approach, they decelerate due to interfacial tension, reaching their maximum velocity, known as terminal velocity. In the figure, the 3.9 mm Al$_2$O$_3$ particles have a terminal velocity of about 0.135 m/s, while the 3.1 mm Al$_2$O$_3$ particles reach around 0.10 m/s. For PP particles, the 3.1 mm size achieves about 0.035 m/s, and the 3.9 mm size reaches approximately 0.08 m/s. The comparison highlights that particle size significantly influences terminal velocity, with larger Al$_2$O$_3$ particles and PP particles exhibiting greater terminal velocities than their smaller counterparts.

4. Discussion

In this study, a particle floating experiment was conducted in a rectangular water tank with a controllable flow rate. Two different viscosity silicone oils with viscosities of 0.0288 Pa·s and 0.0096 Pa·s were used to simulate the slag phase, and two different wettability and diameter PP particles and hollow Al$_2$O$_3$ particles were used to simulate inclusions. This study simulated the movement of inclusions at the slag-steel interface and established a particle floating

motion model based on Newton's second law to explore the process of inclusion floating and being adsorbed and removed by inclusions.

1) When the sink fluid is stationary, when simulating with silicone oil with a viscosity of 0.0288 Pa·s, the dimensionless displacement of the hollow Al$_2$O$_3$ particles with a diameter of 3.93 mm is about 1.0 mm, while the dimensionless displacement of the PP particles with a diameter of 3.96 mm is about 0.7 mm. The dimensionless displacement of the hollow Al$_2$O$_3$ particles is greater than that of the PP particles. When simulating with silicone oil with a viscosity of 0.0096 Pa·s, the dimensionless displacement of the hollow Al$_2$O$_3$ particles with a diameter of 3.12 mm is about 0.8 mm, and the dimensionless displacement of the PP particles with a diameter of 3.13 mm is about 1.25 mm. The dimensionless displacement of the hollow Al$_2$O$_3$ particles is less than that of the PP particles. This is because the PP particles show better wettability when the viscosity of the silicone oil is low.

2) When the fluid flows, the dimensionless displacements of Al$_2$O$_3$ particles with a diameter of 3.9 mm and Al$_2$O$_3$ particles with a diameter of 3.1 mm are 0.75 mm and 0.65 mm, respectively.

The larger the particle diameter, the greater the dimensionless displacement. The dimensionless displacements of PP particles with diameters of 3.9 mm and 3.1 mm are 1.7 mm and 0.45 mm, respectively. The larger the particle diameter, the greater the dimensionless displacement.

3) When the water tank fluid is stationary and the viscosity of the silicone oil is 0.0096 Pa·s, the terminal velocities of Al_2O_3 particles with a diameter of 3.12 mm and Al_2O_3 particles with a diameter of 3.93 mm are 0.135 m/s and 0.143 m/s, respectively. The larger the particle diameter, the greater its terminal velocity. The terminal velocities of PP particles with a diameter of 3.13 mm and 3.96 mm are 0.125 m/s and 0.122 m/s, respectively, and the particle diameter has little effect on the terminal velocity. For Al_2O_3 particles with poor wettability, the particle diameter has a great influence on the particle's terminal velocity, while for particles with good wettability, the particle diameter has a slight effect on the particle's terminal velocity.

4) In the actual production process, inclusion removal is a key issue in steelmaking. Inclusion removal usually includes three steps. The first step is to float to the steel-slag interface, the second step is to pass through the steel-slag interface, and the third step is the dissolution of inclusions in the slag layer. This study focuses on the second step of inclusions passing through the steel-slag interface, which is also the key to whether inclusions can be successfully removed. Through the results of this experimental study, it can be concluded that the larger the particle diameter, the greater its dimensionless displacement, and the size of the inclusion diameter plays an important role in inclusion removal. Because as the size of the inclusion increases, the buoyancy has a greater effect on it than the surface tension. This experiment can well obtain the actual situation of the interface and qualitatively describe the movement process of inclusions passing through the steel-slag interface.

5. Conclusion

Using a high-speed camera and motion analysis software, we investigated how variations in particle size, density, and oil viscosity affect the movement of PP and hollow Al_2O_3 particles at the water-oil interface under both static and dynamic conditions, modeling the floating dynamics essential in steelmaking processes.

Key findings show that, although having lower densities than water and silicone oil, PP and hollow Al_2O_3 particles are preferentially stable at the water-oil interface under static conditions. In silicone oil with a viscosity of 0.0288 Pa·s, smaller PP particles (3.96 mm) displaced about 0.7 of dimensionless displacement, whereas bigger hollow Al_2O_3 particles (3.93 mm) displaced around 1.0 of dimensionless displacement. Dynamic studies revealed that larger particles traveled further during specific periods, demonstrating the role of particle size in floating dynamics.

These findings have important implications for improving inclusion control techniques in steelmaking. Manufacturers can improve the efficiency of inclusion removal processes by understanding how particle characteristics influence their behavior at the interface, resulting in higher steel quality and production efficiency.

Recommendations

Future research should look into the interplay of particle surface characteristics, such as wettability and interaction with surfactants, to improve simulation models' predictive capabilities. Furthermore, studying the effects of operational characteristics such as temperature changes and flow dynamics could provide detailed insights into real-world smelting circumstances.

Ethical Statement

This study does not contain any studies with human or animal subjects performed by any of the authors.

Conflicts of Interest

The authors declare that they have no conflicts of interest to this work.

Data Availability Statement

Data available on request from the corresponding author upon reasonable request.

Author Contribution Statement

Sajjad Muhammad: Investigation, Writing – original draft. **Xin Tao:** Software, Validation, Formal analysis, Data curation, Writing – original draft, Writing – review & editing. **Dekang Ren:** Data curation, Visualization. **Hongyu Zhang:** Software, Validation, Investigation. **Tao Liu:** Software, Investigation, Data curation. **Chao Chen:** Conceptualization, Methodology, Resources, Writing – review & editing, Supervision, Project administration.

References

[1] Kiessling, R. (1968). *Non-metallic inclusions in steel: Part III: The origin and behavior of inclusions and their influence on the properties of steels*. UK: The Metals Society.

[2] Jiang, M., Liu, J. C., Li, K. L., Wang, R. G., & Wang, X. H. (2021). Formation mechanism of large CaO-SiO_2-Al_2O_3 inclusions in Si-deoxidized spring steel refined by low basicity slag. *Metallurgical and Materials Transactions B, 52*, 1950–1954.

[3] Podder, A., Coley, K. S., & Phillion, A. B. (2022). Modeling study of steel–slag–inclusion reactions during the refining of Si–Mn killed steel. *Steel Research International, 94*, 2100831.

[4] Podder, A., Coley, K. S., & Phillion, A. B. (2024). Simulation of ladle refining reactions in Si–Mn-killed steel. *Steel Research International, 95*, 2300330.

[5] Gutiérrez, E., Garcia-Hernandez, S., & Barreto, J. J. (2019). Mathematical analysis of the touching inclusions parameters at the tundish free surface to predict more realistic inclusion removal rates. *Steel Research International, 90*, 1900328.

[6] Guo, X. P., Godinez, J., Walla, N. J., Silaen, A. K., Oltmann, H., Thapliyal, V., . . . , & Zhou, C. Q. (2021). Computational investigation of inclusion removal in the steel-refining ladle process. *Processes, 9*, 1048.

[7] Li, X., Hu, S., Wang, D., Qu, T., Wu, G., Zhang, P., . . . , & Zhang, Z. (2022). Inclusion removements in a bottom-stirring ladle with novel slot-porous matched dual plugs. *Metals, 12*, 162.

[8] Li, X., Wang, D., Tian, J., Wang, H., Qu, T., Hou, D., . . . , & Wu, G. (2024). Modeling of bubble transportation, expansion, as well as adhesion of inclusions in a ladle with different tuyeres. *Metallurgical and Materials Transactions B, 55*, 14–31.

[9] Siddiqui, M. I. H., Albaqami, A., Arifudin, L., Alluhydan, K., & Alnaser, I. A. (2022). Simulation of inclusion particle motion behavior under interfacial tension in continuous casting mold. *Materials*, *15*, 7458.

[10] Siddiqui, M. I. H., Arifudin, L., Alnaser, I. A., Ali, M. A., & Alluhydan, K. (2023). Modeling of interfacial tension and inclusion motion behavior in steelmaking continuous casting mold. *Materials*, *16*, 968.

[11] Cejka, J., & Michelic, S. K. (2023). In-situ observation of steel/slag/inclusion interaction by means of high-temperature confocal scanning laser microscopy. *Metals*, *13*(4), 686.

[12] Wang, R., Li, Y. H., Li, D. Z., Kang, Y., Bao, Y. P., & Yan, Z. J. (2020). Inclusions absorbed by slags in interstitial-free steel production. *Steel Research International*, *91*, 1900440.

[13] Yeo, S., Um, H., & Chung, Y. (2021). Alumina activity on dissolution behavior of alumina particles in CaO-Al$_2$O$_3$-SiO$_2$ slags. *Metallurgical and Materials Transactions B*, *52*, 3938–3945.

[14] Wen, X., Ren, Y., & Zhang, L. F. (2022). Effect of CaF$_2$ contents in slag on inclusion absorption in a bearing steel. *Steel Research International*, *94*, 2200218.

[15] Wikström, J., Nakajima, K., Jonsson, L., & Jönsson, P. (2008). Application of a model for liquid inclusion separation at a steel-slag interface for laboratory and industrial situations. *Steel Research International*, *79*, 826–834.

[16] Chen, C., Ni, P. Y., Jonsson, L. T. I., Tilliander, A., Cheng, G. G., & Jönsson, P. G. (2016). A model study of inclusions deposition, macroscopic transport, and dynamic removal at steel–slag interface for different tundish designs. *Metallurgical and Materials Transactions B*, *47*, 1916–1932.

[17] Hu, Z. Y., Duan, H. J., & Zhang, L. F. (2022) Detachment mechanism of inclusions from the interface between molten steel and slag. *Metallurgical and Materials Transactions B*, *53*, 1339–1343.

[18] Sun, Y. P., Duan, H. J., & Zhang, L. F. (2023). A boundary layer model for capture of inclusions by steel–slag interface in a turbulent flow. *Journal of Iron and Steel Research International*, *30*, 1101–1108.

[19] Nakajima, K., & Okamura, K. (1992). Inclusion transfer behavior across molten steel-slag interface. In *Proceedings of the 4th International Conference on Molten Slags and Fluxes*, 505–510.

[20] Xuan, C. J., Persson, E. S., Sevastopolev, R., & Nzotta, M. (2019). Motion and detachment behaviors of liquid inclusion at molten steel-slag interfaces. *Metallurgical and Materials Transactions B*, *50*, 1957–1973.

[21] Liu, W., Liu, J., Zhao, H. X., Yang, S. F., & Li, J. S. (2021). CFD modeling of solid inclusion motion and separation from liquid steel to molten slag. *Metallurgical and Materials Transactions B*, *52*, 2430–2440.

[22] Zhang, X. M., Pirker, S., & Saeedipour, M. (2023). Numerical investigation of particle motion at the steel–slag interface in continuous casting using VOF method and dynamic overset grids. *Experimental and Computational Multiphase Flow*, *5*, 178–191.

[23] Cao, J., Li, Y., Lin, W., Che, J., Zhou, F., Tan, Y., & Chen, C. (2023). Assessment of inclusion removal ability in refining slags containing Ce$_2$O$_3$. *Crystals*, *13*(2), 202.

[24] Zhao, J., Zhu, H., Chen, J., Wang, L., Yan, X., & Sun, J. (2024). Numerical simulation on the motion behavior of micro-inclusions at the steel–slag interface. *Metallurgical and Materials Transactions B*, *55*, 1700–1711.

[25] Valdez, M., Shannon, G. S., & Sridhar, S. (2006). The ability of slags to absorb solid oxide inclusions. *ISIJ International*, *46*, 450–457.

[26] Xuan, C. J., & Mu, W. Z. (2020). A mechanism theory of dissolution profile of oxide particles in oxide melt. *Journal of the American Ceramic Society*, *104*, 57–75.

[27] Xuan, C. J., & Mu, W. Z. (2020). Dissolution kinetics of arbitrarily-shaped alumina in oxide melt: An integration of phase-field modelling and real-time observation study. *Journal of Alloys and Compounds*, *834*, 155168.

[28] Ferchichi, Y., & Duval, H. (2011). Physical modeling of inclusion approach to the steel-slag interface with focus on hydrodynamic interactions. *Advanced Engineering Materials*, *13*, 550–555.

[29] Liu, C., Yang, S. F., Li, J. S., Zhu, L. B., & Li, X. G. (2016). Motion behavior of nonmetallic inclusions at the interface of steel and slag. Part I: Model development, validation, and preliminary analysis. *Metallurgical and Materials Transactions B*, *47*, 1882–1892.

[30] Zhou, Y. L., Deng, Z. Y., & Zhu, M. Y. (2017). Study on the separation process of non-metallic inclusions at the steel−slag interface using water modeling. *International Journal of Minerals, Metallurgy, and Materials*, *24*, 627–637.

[31] Zhu, Y. L., Li, T., Tang, G. Z., Gu, Y. J., & Cui, H. N. (2022).Water model study on the flotation behaviors of inclusion clusters in molten steel. *ISIJ International*, *62*(7), 1408–1417.

[32] Zhu, Y. L., Cui, H. N., Li, T., Tan, M., Tang, G. Z., Xin, Z. Y., & Xiao, T. T. (2023). Study on the motion behavior of inclusion clusters at the steel–slag interface. *Metallurgical and Materials Transactions B*, *54*, 101–114.

[33] Nishibata, H., Miyatake, T., Matsuda, Y., Uddin, M. A., Kato, Y., & Harada, A. (2024). Effect of wettability, number of liquid phases, and agitation procedure on agglomeration/breakup/transfer of fine particles in liquid. *Steel Research International*, *95*, 2300331.

[34] Tao, X., Cao, J. Q., Wang, J., He, X. N., Meng, L. Y., Guo, Y. B., . . . , & Chen, C. (2024). Physical model of inclusions removal at static steel–slag interface. *Materials*, *17*, 2244.

[35] Liu, Y., Cheng, S., & Liu, T. (2024). Study of inclusions-removal and slag-metal dispersion phenomenon in gas-stirred ladle. *International Journal of Chemical Reactor Engineering*, accepted paper.